Studies of the Ground and Excited-State Surfaces of the Retinal Chromophore using CAM-B3LYP

Ivan V. Rostov,[†] Roger D. Amos,*[,†] Rika Kobayashi,[†] Giovanni Scalmani,[‡] and Michael J. Frisch[‡]

Australian National University Supercomputer Facility, Mills Road, Canberra, ACT 0200, Australia, and Gaussian, Inc., 340 Quinnipiac Street, Building 40, Wallingford, Connecticut 06492

Received: November 29, 2009; Revised Manuscript Received: January 22, 2010

The isomerization of the 11-cis isomer (PSB11) of the retinal chromophore to its all-trans isomer (PSBT) is examined. Optimized structures on both the ground state and the excited state are calculated, and the dependence on torsional angles in the carbon chain is investigated. Time-dependent density functional theory is used to produce excitation energies and the excited-state surface. To avoid problems with the description of excited states that can arise with standard DFT methods, the CAM-B3LYP functional was used. Comparing CAM-B3LYP with B3LYP results indicates that the former is significantly more accurate, as a consequence of which detailed cross sections of the retinal excited-state surface are obtained.

1. Introduction

Rhodopsin is the retinal protein located in the cell membrane and serving as the photoreceptor in the rod cells of vertebrate eyes. The chromophore of rhodopsin is the retinal molecule embedded in a cavity and covalently bound via a protonated Schiff base (PSB) linkage to the ε-amino group of lysine side chain.[1] The chromophore serves two major functions. First, it traps the photons hitting the eye retina. Second, it relays this energy into conformational changes that activate the protein stepwise toward G-protein coupling.[2] The process starts when the energy of the photon gained by the chromophore triggers a rapid multistep photoisomerization in which the 11-cis isomer of the retinal (PSB11) is converted to the all-trans isomer (PSBT); see Figure 1. This is considered the primary event in vision. The retinal photoisomerization process has been studied in recent years by high-resolution methods such as femtosecond spectroscopy,[3−6] femtosecond-stimulated Raman spectroscopy (FSRS),[7−10] coherent anti-Stokes Raman scattering (CARS)[11,12] and Fourier transformed optical absorption (FTOA).[13] These experimental techniques established that the first step of the PSB11 → PSBT isomerization is complete in 200 fs, has a quantum yield of 0.67 and results in a photoproduct that stores 35 kcal/mol of the incident photon energy.[4,10,14] This primary photoproduct of rhodopsin, called photorhodopsin, has been identified by its red-shifted absorption maximum with $\lambda_{max} \sim$ 570 nm versus $\lambda_{max} \sim$ 480 nm for rhodopsin.[4,14] Photorhodopsin thermally decays to form bathorhodopsin with $\lambda_{max} \sim$ 540 nm in ∼ 5 ps.[4,15−17] In its turn, bathorhodopsin decays through a series of intermediates leading to the deprotonation of the retinal Schiff base and triggering of the G-protein cascade.[10]

The primary objective of this study is to understand the initial step of photoisomerization, i.e., the PSB11 → PSBT isomerization. In particular, the key questions, which have not been answered even by such advanced experimental techniques as listed above, are, what is the molecular structure of the chromophore in the photorhodopsin and bathorhodopsin states, and how does the molecular structure of retinal chromophore evolve on the way from rhodopsin to photorhodopsin and, then, to bathorhodopsin?

It is hoped that advanced computational methods can shed light on the mechanisms of this rapid photoisomerization process. The nature of the system means that the method of choice must have the capacity to deal with electronic excitations, including geometry optimizations, and must also include electron correlation. As such, one can use either methods based on the configuration interaction (CI) theory, such as CASSCF, CASPT2/CASSCF, CC2, SORCI, and MRCISD, or the time-dependent density functional theory[18,19] (TD DFT) methods. In fact, both approaches have been applied already to PSB to elucidate the photoisomerization process (see refs 20−26 for CASSCF and post-CASSCF calculations, refs 27−29 for CC2, refs 30 and 31 for SORCI, refs 24 and 31 for MRCISD, and refs 20, 24, 27−30, and 32−36 for TD DFT studies of the retinal chromophore or its homologues).

The computational costs of high-accuracy methods based on the CI theory rise drastically with molecular size. This imposes some limits on their applicability toward the chromophore retinal studies. So far, either they have been used in single-point excited-state calculations with geometry obtained by some other means, e.g., ground-state optimized geometries, or they have been used in more systematic studies of some smaller model systems mimicking the retinal PSB molecule in the region adjacent to the $C_{11}-C_{12}$ bond. The TD DFT method is not as expensive as the CASSCF or CC2 methods, and its computational costs are similar to CIS. This makes TD DFT, especially after the formulation and implementation of analytic expressions for excited-state energy gradients,[37,38] capable of producing a more systematic exploration of energy profiles for the excited states of rhodopsin, i.e., with all coordinates of the retinal chromophore molecule included in an excited-state energy minimization.

The drawback of TD DFT theory is in the approximate nature of the DFT functionals. In particular, the unphysical long-range asymptote of the exchange part of popular functionals, e.g., B3LYP[39,40] makes them unsuitable for calculations of excited states having a large charge-transfer (CT) component.[41,42] The retinal PSB11 chromophore excitation $S_0 \rightarrow S_1$ is found to have

[†] Australian National University Supercomputer Facility.
[‡] Gaussian, Inc.

10.1021/jp911329g
Published on Web 04/06/2010

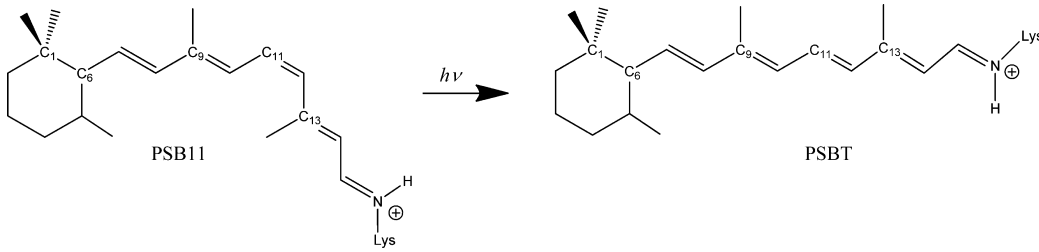

Figure 1. PSB11 → PSBT photoisomerization of the retinal PSB.

a substantial contribution from the charge-transfer bands.[21,43−45] Therefore, all TD DFT results for the retinal chromophore published so far[20,24,27−30,32−36] must be considered with caution. However, it should be emphasized that it is not TD DFT theory itself that is the reason for failure, as has been concluded by some authors,[29,30] but rather the incapacity of the popular DFT potentials to deal accurately with charge-transfer states.

The appearance of the CAM-B3LYP hybrid functional with its more correct long-range asymptote[42,46] and encouraging results of its use in TD DFT calculations of excited states with a large charge-transfer component in various kinds of molecular systems, e.g., refs 47−51, has made it a natural candidate for application to this problem. This paper presents the results of a systematic study of the S_0 and S_1 energy surfaces of the retinal PSB molecule in vacuo using TD DFT with the CAM-B3LYP functional for the purpose of revealing the mechanism of the first steps of the photoisomerization.

The effects of the protein environment on the photoisomerization process, though of importance, have been left out of the present study. Recent publications by various authors,[22,24−26,31,35,36,52−58] in which the protein has been included for consideration via the QM/MM approach are recommended for further reading on this topic.

2. Computational Details

2.1. CAM-B3LYP Functional. Briefly, CAM-B3LYP combines the features of hybrid functionals such as B3LYP[39,40] with the long-range corrected functionals of Hirao et al.[42] The exchange functional is a mixture of exact, i.e., Hartree−Fock, and DFT exchange, but unlike B3LYP, the ratio of exact to DFT exchange varies in different regions of the molecule. This is achieved by partitioning the two-electron operator according to the formula[46]

$$\frac{1}{r_{12}} = \frac{1 - (\alpha + \beta \cdot \mathrm{erf}(\mu r_{12}))}{r_{12}} + \frac{\alpha + \beta \cdot \mathrm{erf}(\mu r_{12})}{r_{12}} \quad (1)$$

The short-range part of this operator is omitted and replaced by a short-range (or, more precisely, high-density) DFT exchange defined as

$$E_{x\sigma}^{\mathrm{sr}} = -\frac{1}{2}\int \rho_\sigma^{4/3} K_\sigma \left[1 - \alpha - \frac{8}{3}\beta \cdot a_\sigma \left(\sqrt{\pi}\,\mathrm{erf}\left(\frac{1}{2a_\sigma}\right) + 2a_\sigma(b_\sigma - c_\sigma)\right)\right] \mathrm{d}r \quad (2)$$

where

$$a_\sigma = \frac{\mu\sqrt{K_\sigma}}{6\sqrt{\pi} \cdot \rho_\sigma^{1/3}} \quad (3)$$

$$b_\sigma = \exp\left(-\frac{1}{4a_\sigma^2}\right) - 1 \quad (4)$$

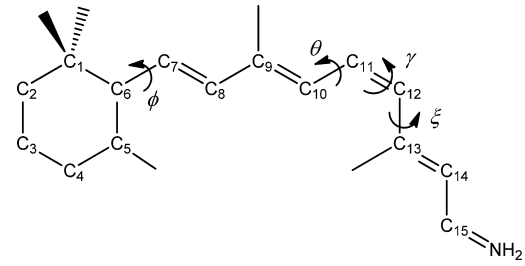

Figure 2. Retinal PSB model and torsional angle notations used in this work.

$$c_\sigma = 2a_\sigma^2 b_\sigma + \frac{1}{2} \quad (5)$$

and K_σ is the original unattenuated exchange functional (in this case Becke88[59]). This expression is numerically unstable at large values of a_σ (small values of ρ), but a stable formula can be obtained by expanding both the exponential and the error function as a power series in a_σ and regrouping the terms.

The degree of mixing of exact and DFT exchange is controlled by the parameters α and β with the proportion of exact exchange increasing from α at short-range to $\alpha + \beta$ at long-range and the DFT exchange decreasing correspondingly. The values of $\alpha = 0.19$ and $\beta = 0.46$, recommended by Yanai et al., have been used. The correlation functional uses the VWN5[60] parametrization of the Local Density Approximation together with the Lee−Yang−Parr (LYP) functional.[61]

2.2. Calculations. The calculations presented in this paper were performed for the PSB retinal molecule in vacuo. The molecule was detached from the Lys-296 residue of rhodopsin and the broken bond was capped by H. In the first stage of the calculations, the ground-state potential energy surface (PES) of the PSB retinal molecule with charge +1 and multiplicity 1 was explored with respect to the four torsional angles shown in Figure 2. The PSB11 → PSBT photoisomerization process passes along the C_{10}−C_{11}=C_{12}−C_{13} torsional angle, making it the major component of the reaction coordinate. The neighboring torsional angles, C_9=C_{10}−C_{11}=C_{12} and C_{11}=C_{12}−C_{13}=C_{14}, can facilitate the photoisomerization process; therefore, they were taken into consideration as well. The fourth coordinate was the C_5=C_6−C_7=C_8 torsional angle, which determines the orientation of the β-ionone ring with respect to the retinal chain. To facilitate comparison with ref 28, the torsional angles are denoted γ(C_{10}−C_{11}=C_{12}−C_{13}), ϕ(C_5=C_6−C_7=C_8), θ(C_9=C_{10}−C_{11}=C_{12}), and ξ(C_{11}=C_{12}−C_{13}=C_{14}). All possible equilibrium conformers of the retinal PSB, with respect to these angles, were located, i.e., scans of the potential surface were made, by varying these angles while simultaneously optimizing all other coordinates. Vertical excitations were then calculated using time-dependent density functional theory (TD DFT).

The next stage of the calculations was the optimization of the molecular structure in the first excited state using TD DFT. The fully relaxed potential-energy curves for the first excited

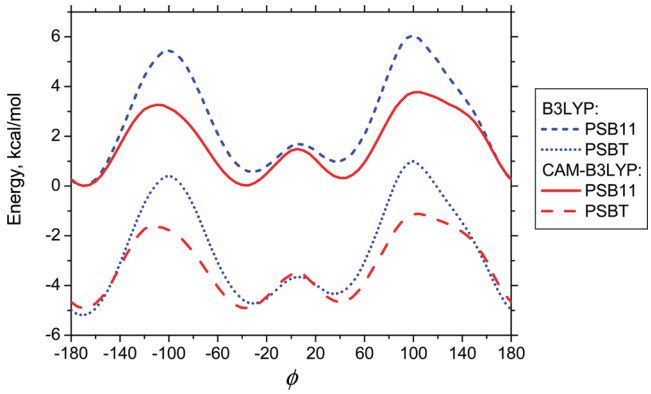

Figure 3. Ground-state potential energy curve for the PSB11 and PSBT conformers of the retinal chromophore as a function of the torsional angle $\phi(C_5{=}C_6{-}C_7{=}C_8)$ calculated at the B3LYP and CAM-B3LYP levels with interval of 10°.

state with respect to the torsional angles were produced. This part of the calculation is of particular interest because the TD DFT first excited-state curves produced with the B3LYP functional, as shown by Send and Sundholm,[28] were significantly different from the results they produced at the CC2 level. This makes these calculation a test case for the CAM-B3LYP functional. As the CAM-B3LYP functional is more appropriate than B3LYP for the CT excited-state calculations, it is expected that the CAM-B3LYP results would be more in agreement with the CC2 results.

All the calculations presented in this paper were carried out with the Gaussian Development Version.[62] Most calculations were done with both B3LYP and CAM-B3LYP. The calculations employing the B3LYP functional were done for verification purposes and basically repeated analogous calculations by Send and Sundholm.[28] A difference, believed to be insignificant, is in the choice of basis set. The present study employed 6-31G(d) in both the ground state and TD DFT calculations, as compared to TZVP in ref 28. Some preliminary tests showed that these two basis sets produce consistent results for this system.

All calculations of the Mulliken atomic charges and dipoles for the excited states have been performed including the relaxation term in the one-particle density matrix.[63,64]

3. Results and Discussion

3.1. Orientation of the β-Ionone Ring. The ground-state (S_0) and first excited (S_1)-singlet-state potential energy surfaces with respect to ϕ, keeping all other coordinates fully relaxed, were produced for both PSB11 and PSBT conformers. This corresponds to the rotation of the β-ionone ring around the single $C_6{-}C_7$ σ-bond. Figure 3 shows the B3LYP and CAM-B3LYP S_0 potential energy curves.

Rotation of the β-ionone ring around the $C_6{-}C_7$ σ-bond (Figure 3) gives three possible conformations: one 6-s-anti- and two 6-s-gauche-. In the literature these are commonly called 6-s-trans and 6-s-cis, respectively. This common notation will be used, keeping in mind that there are two 6-s-cis conformations possible with either negative or positive value of ϕ. These two latter conformations are denoted as 6-s-cis(−) and 6s-cis(+), respectively. Each of the local minima was fully optimized. The orientation of the β-ionone ring has little effect on other torsional angles of interest. All of θ, γ, and ξ remained nearly planar throughout the variation of ϕ. The optimized values of ϕ and γ in the equilibrium ground-state conformations are shown in Table 1. The values of θ and ξ are 180 ± 0.8° for all tabulated conformations.

Using B3LYP, 6-s-trans is the most favorable orientation of the β-ionone ring for both 11-cis and all-trans retinal PSB structures. CAM-B3LYP, compared to B3LYP, stabilizes the 6-s-cis ground-state energy by 0.5−0.6 kcal/mol, particularly for 6-s-cis(−) which corresponds to the experimentally observed structure for retinal embedded in protein. This makes the CAM-B3LYP 6-s-cis(−) energy lower than (in the case of the all-trans structure) or nearly equal to (cf. 11-cis structure) the corresponding 6-s-trans energies. The calculated value of ϕ (−31.9° with B3LYP, −37.6° with CAM-B3LYP) for the 6-s-cis-11-cis conformation in the ground state is in agreement with experimental values of ϕ for PSB11 (−30.3°, −31.9°,[57] and −44°[53]). For this reason, the 6-s-cis(−) orientation of the β-ionone ring was adopted for all subsequent calculations, when potential energy curves were calculated with respect to other torsional angles.

The S_0 potential energy curves with respect to ϕ calculated with B3LYP and CAM-B3LYP have no major differences. The situation is significantly different for the S_1 potential energy curves.

The full geometry optimization of PSB11 in the first excited state using the TD DFT method with the B3LYP functional produces structures with the β-ionone ring nearly perpendicular to the retinal plane. The TD DFT B3LYP potential-energy curves calculated for the first excited state of PSB11 with respect to ϕ form two equally deep minima at $\phi = -90°$ and +94°, as shown in Figure 4a. In the regions between −35° and +35° and beyond ±155° the B3LYP energy difference between the HOMO and LUMO is too small. This makes the S_0 and S_1 states, calculated for the S_1-optimized geometry, nearly degenerate. In turn, this makes convergence in the S_1 geometry optimization nearly impossible due to the S_0 and S_1 states being interchangeable.

In contrast, TD DFT calculations of the S_1 potential-energy curve (see Figure 4b) employing the CAM-B3LYP functional had no such a problem, as the gap between HOMO and LUMO in these calculations remained quite considerable along the full course of twist in ϕ. The CAM-B3LYP S_1 potential energy curve for PSB11 contains five local minima in the full course of the ϕ revolution. Three of the S_1 minima, at −32°, +37°, and −171°, have analogues on the S_0 curve. Another two, at −86° and +95°, can be associated with two produced in the analogous S_1 TD DFT B3LYP calculations. The barrier for the transition from the global S_1 6-s-cis minimum ($\phi = -32°$) to the twisted β-ionone ring S_1 minimum ($\phi = -86°$) is ∼3 kcal/mol with the latter higher in energy by ∼2.3 kcal/mol than the former. Therefore, the TD DFT CAM-B3LYP results suggest that the PSB11 chromophore would not have any preference for the perpendicular orientation of the β-ionone ring at any point along the photoisomerization path. In this respect, TD DFT CAM-B3LYP results are consistent with CC2 calculations done by Send and Sundholm.[28] Moreover, the results do not support the point of view that the orientation of the β-ionone ring, located five bonds away from the $C_{11}{=}C_{12}$ bond plays a decisive role in the PSB11 → PSBT isomerization. As a check, the energies of the stationary points were recalculated at the optimized 6-31G* geometries using a larger 6-311G(2d,p) basis set. The results, also in Table 1, show no significant change from the smaller basis set.

3.2. Vertical Excitations of PSB11 and PSBT. Tables 2 show vertical excitation energies and oscillator strengths at the ground-state PSB11 and PSBT minima calculated with the TD

TABLE 1: B3LYP and CAM-B3LYP Ground-State E_0 Energies, Values of ϕ and γ for PSB11 and PSBT Conformations of the Retinal PSB Chromophore with Varying Orientations of the β-Ionone Ring[a]

conformation	ϕ, deg	γ, deg	S_0, kcal/mol 6-31G(d)[b]	S_0, kcal/mol 6-311G(2d,p)[b]
		B3LYP Results		
6-s-cis(−)-11-cis	−31.9	0.2	0.0	0.0
6-s-cis(+)-11-cis	37.4	2.0	0.4	0.4
6-s-trans-11-cis	−170.2	0.7	−0.6	−0.7
6-s-cis(−)-all-trans	−30.8	179.9	−5.3	−5.5
6-s-cis(+)-all-trans	35.4	−179.9	−4.9	−5.1
6-s-trans-all-trans	−170.8	179.9	−5.8	−6.1
CAM-B3LYP Results				
6-s-cis(−)-11-cis	−37.6	0.2	0.0	0.0
6-s-cis(+)-11-cis	42.0	1.5	0.3	0.3
6-s-trans-11-cis	−169.1	0.6	0.0	−0.1
6-s-cis(−)-all-trans	−36.1	179.9	−5.0	−5.2
6-s-cis(+)-all-trans	40.9	−179.9	−4.7	−4.9
6-s-trans-all-trans	−169.6	179.7	−4.8	−5.2

[a] Each conformer was completely optimized using the 6-31G(d) basis set. Additional single point energy evaluations used the 6-311G(2d,p) basis set. [b] The energy scale is shifted to make the S_0 energy of 6-s-cis(−)-11-cis (PSB11) conformer as 0.

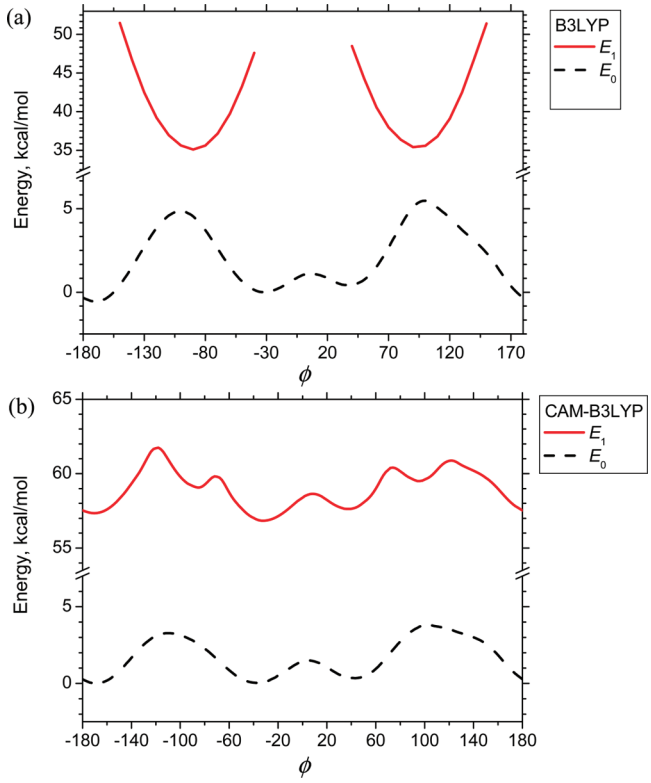

Figure 4. Potential-energy curves for the ground (E_0) and first excited (E_1) states of the PSB11 chromophore as functions of the ϕ angle calculated at the DFT (E_0) and TD DFT (E_1) levels with interval of 10° using the B3LYP (a) and CAM-B3LYP (b) functionals.

DFT method using B3LYP and CAM-B3LYP functionals. The vertical S_1 excitation of PSB11 measured in vacuo[65] is 2.03 eV. In the experiment the molecule had terminating methyl groups on the nitrogen, rather than hydrogens, which is known to lower the excitation energy slightly,[27] so the corresponding result with terminating hydrogens would be ∼2.1 eV. There are also measurements in solvent, but these are considerably higher.[14,66,67]

Ab initio calculations using correlated methods such as CASPT2 or CC2 give S_1 excitation energies in the range 1.9−2.4 eV depending on the basis set and geometry, with those calculations using large basis sets, e.g., refs 27 and 68, giving 2.1−2.2 eV, in good agreement with experiment. The TD DFT calculations reported here with DFT-optimized geometries overestimate the S_1 vertical excitation energy by ∼0.4 eV for CAM-B3LYP/6-31G(d). The tendency of CAM-B3LYP to give excitation energies slightly higher than CASPT2 or CC2 has been noted before.[48] However, the main focus of this study is the shape of the excited-state PE curve, and this is probably at least qualitatively correct.

3.3. Rotation about the C_{11}=C_{12} Bond. The major coordinate in the PSB11 → PSBT isomerization is the torsional angle γ. Its variation corresponds to the twist of the C_{11}=C_{12} bond. The S_0 profile $E_0(\gamma)$ forms two minima corresponding to PSB11 and PSBT conformations, as shown in Figure 5. As in the case of $E_0(\phi)$, the B3LYP and CAM-B3LYP $E_0(\gamma)$ curves are nearly identical. Both functionals give the PSBT S_0 conformation as being lower in energy than the PSB11 S_0 by ∼5.0 kcal/mol. The minima are separated by a high barrier of ∼20 kcal/mol for the adiabatic PSB11 → PSBT transition.

This similarity observed in the comparison of B3LYP and CAM-B3LYP $E_0(\gamma)$ results completely disappears on proceeding to the analysis of the S_1 potential-energy TD DFT curves (E_1). In the B3LYP case (Figure 5a), the $E_1(\gamma)$ curve repeats in shape the $E_0(\gamma)$ curve with the same two minima corresponding to the PSB11 and PSBT conformations. The E_1(PSBT) B3LYP minimum is lower than the E_1(PSB11) minimum by 5.6 kcal/mol and the barrier for the S_1(PSB11) → S_1(PSBT) transition is ∼23 kcal/mol. The TD DFT B3LYP energy for the vertical excitation in the S_0(PSB11) configuration is 2.36 eV = 54.4 kcal/mol. The energy of relaxation after vertical excitation to the S_1(PSB11) minimum is 0.83 eV = 19.18 kcal/mol. As discussed in the previous section, the B3LYP S_1(PSB11) minimum has the β-ionone ring oriented perpendicularly to the retinal chain.

The TD DFT CAM-B3LYP $E_1(\gamma)$ curve (Figure 5b) is very different from its B3LYP counterpart. The only similarity is that it too has PSB11 and PSBT minima with the E_1(PSB11) − E_1(PSBT) CAM-B3LYP energy difference of 4.6 kcal/mol. However, in the case of CAM-B3LYP, the E_0 and E_1 curves demonstrate avoided crossing (AC) regions around $\gamma = \pm 90°$ forming two more, much deeper, minima on the $E_1(\gamma)$ curve. It should be noted that, although these minima are described as avoided crossing regions, there should be a conical intersection with the ground state somewhere in these region. Its precise position has not been located however. The values of γ calculated at these minima were 92.7°and −92.9°. The CAM-B3LYP vertical excitation energy for the S_0(PSB11) configuration is 2.53 eV = 58.4 kcal/mol. The energy of relaxation

TABLE 2: Vertical S_1 Excitation Energies and Oscillator Strengths for the Ground-State Optimized Structures[a]

method	conformation	S_1, eV	S_1, nm	f	S_2, eV	S_2, nm	f
TD DFT, B3LYP	PSB11	2.36	526	1.21	3.17	392	0.49
TD DFT, B3LYP	PSBT	2.39	520	1.51	3.17	391	0.48
TD DFT, CAM-B3LYP	PSB11	2.53	490	1.43	3.70	335	0.37
TD DFT, CAM-B3LYP	PSBT	2.54	489	1.75	3.69	336	0.34
exp (in MeOH)[14,67]	PSB11-n-Bu	2.79/2.82	445/440				
exp (in vacuo)[65]	PSB11-$(CH_3)_2$	2.03	610		3.18	390	

[a] The S_0 geometry has been optimized with the same functional as in the tabulated TD DFT calculations of vertical excitation energies.

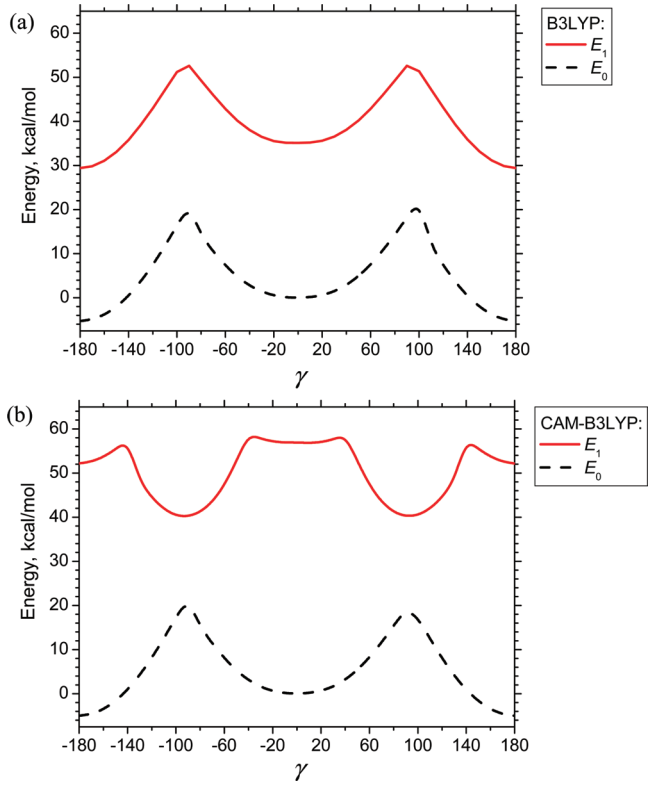

Figure 5. Potential-energy curves for the ground- (E_0) and first excited (E_1) states of the retinal chromophore as functions of the γ angle calculated at the DFT (E_0) and TD DFT (E_1) levels with interval of 10° using the B3LYP (a) and CAM-B3LYP (b) functionals.

after vertical excitation to the E_1(PSB11) minimum is only 1.5 kcal/mol. The orientation of the β-ionone changes a little during the relaxation, according to the CAM-B3LYP results, with ϕ changed from −37.6° (PSB11, S_0, CAM-B3LYP) to −31.6° (PSB11, S_1, CAM-B3LYP). However, the excitation weakens the $\pi-\pi$ bonding between C_{11} and C_{12} and S_1 relaxation brings a noticeable initial twist of the C_{11}═C_{12} bond with γ changed from 0.2° (PSB11, S_0, CAM-B3LYP) to 10.7° (PSB11, S_1, CAM-B3LYP). To get from the S_1 PSB11 minimum to the S_1 AC minimum, the retinal PSB system has still to get over a comparatively small barrier of ∼2 kcal/mol on the $E_1(\gamma)$ curve, upon crossing of which (at $\gamma \sim \pm 45°$) the character of the bond between C_{11} and C_{12} atoms quickly turns from the double bond to the single bond. The freed π-electrons immediately form π-bonds with neighboring carbon atoms. Overall, this causes a major change in character of the bonds in the region between the C_8 and C_{13} atoms of the retinal chain, with the order of single and double bonds being inverted. The plot in Figure 6 illustrates this for three most noticeably changed bonds.

Overall, the most changed is the bond length between C_{11} and C_{12} atoms, which goes from 1.39 Å (double bond) in the PSB11 S_1 retinal configuration to 1.47 Å (single bond) in the AC S_1 minimum. The magnitude of changes in bond lengths gradually fades out when moving away from the C_{11}═C_{12} bond, see Figure 7. No noticeable changes have been observed for bond lengths beyond the C_8 and C_{13} atoms.

Upon reaching either of the S_1 AC minima, the retinal PSB structure loses 16.7 kcal/mol of energy versus the relaxed S_1 PSB11 minimum. A summary of the energies, key bond distances, and torsional angles in S_0 and S_1 minima related to the PSB11 → PSBT retinal PSB transformation is given in Table 3. Some additional values calculated with a larger 6-311G(2d,p) basis are also included.

Analysis of the two lowest excited states, S_1 and S_2, produced in the TD DFT calculations with CAM-B3LYP shows that both of them contain locally excited (LE) and charge-transfer (CT) contributions. The charge distribution and the dipole moment shift for the S_1 and S_2 states are shown in Table 4. As seen from comparison of the Mulliken charge distribution and the dipole moment shift, the LE band prevails for both the S_1 and S_2 states in the 11-cis S_0 and S_1 PSB configurations. On the vertical excitation there is a slight shift of electron density away from the ring. The initial relaxation of the PSB11 S_1 structure, immediately after the vertical excitation, does not result in any large changes in the molecular charge distribution. Direct experimental measurements of the excited-state dipole are only available in solution,[69] and are believed to be significantly different from the gas phase values. The AC region for the S_1 state is characterized by a strong localization of electron charge on the β-ionone end. Consequently, the first excited state S_1 in the AC region has a large CT contribution with a dipole shift $|\mu(S_1) - \mu(S_0)|$ of 21.6 debye. This large change associated with the reorganization of the bonding pattern. There are no experimental estimates of the dipole moment in this region.

The change in nature of the S_1 and S_2 excited states on the path from PSB11 to the AC region can not be tracked by looking at their largest components in terms of MO → MO excitations. Formally, the largest contributions to S_1 and S_2 remain unchanged. It is the HOMO → LUMO excitation for S_1 and the HOMO−1 → LUMO for S_2, with a CI coefficient of ∼0.7 in both cases. However, the molecular orbitals involved in these excitations are changing themselves with twist in γ. Figure 8 shows HOMO−1, HOMO, and LUMO at $\gamma \cong 0°$ and $\gamma \cong 90°$ points of the $E_1(\gamma)$ minimum energy path. It was found that the B3LYP and CAM-B3LYP MOs are nearly identical for the PSB11 S_0 configuration. In contrast, in areas of the perpendicular twist in γ, the B3LYP and CAM-B3LYP HOMO−1, HOMO, and LUMO have a completely different appearance.

In these areas, i.e., for $\gamma \sim \pm 90°$, B3LYP gives a HOMO localized on the β-ionone ring and the LUMO localized on the retinal chain. Therefore, the B3LYP S_1 corresponds to the electron density moving away from the β-ionone ring. In other words, the B3LYP S_1 can be characterized by the positively charged β-ionone ring. Its perpendicular orientation to the retinal chain, free of any kind of π-bonding, only facilitates such an even charge distribution.

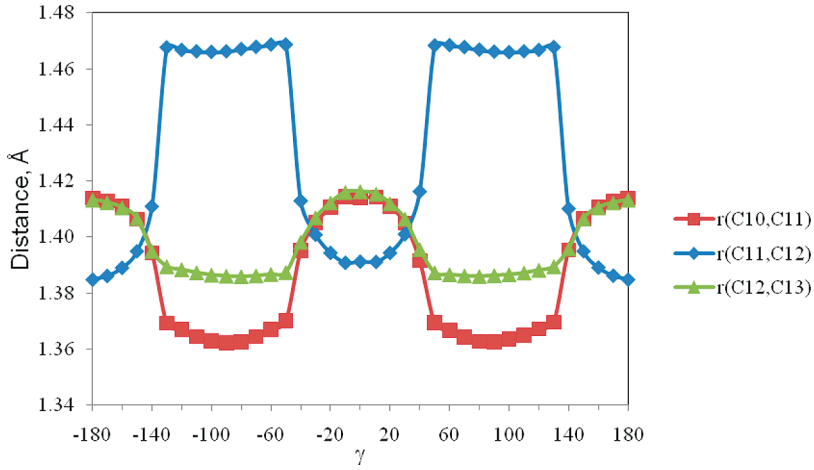

Figure 6. Dependence of bond lengths of the S_1 retinal PSB structure on value of the scanned γ angle in the TD DFT CAM-B3LYP calculations.

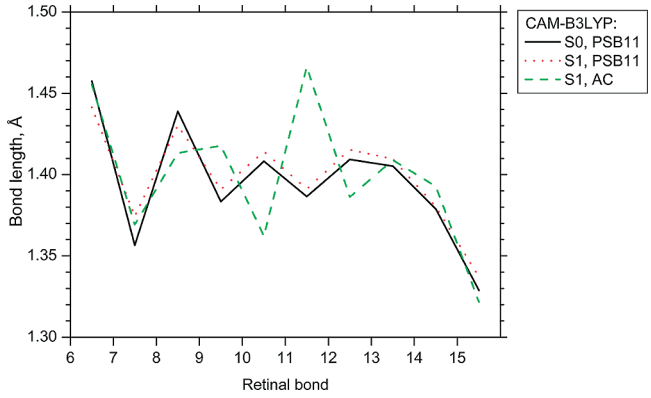

Figure 7. Comparison of the bond-length alternation of the retinal PSB structure in the PSB11 S_0, PSB11 S_1, and one of the AC S_1 ($\gamma = -92.7°$) minima calculated at the TD DFT CAM-B3LYP level. The bond lengths are given between the integers labeling the corresponding atoms.

The CAM-B3LYP HOMO and LUMO isodensity surfaces built for the retinal structure in the AC areas ($\gamma \cong \pm 90°$) are completely different from their B3LYP counterparts. The CAM-B3LYP HOMO is largely localized on the retinal chain closer to the imine terminal group. The CAM-B3LYP LUMO is localized partly on another end of the retinal chain and partly on the β-ionone ring. Overall, it makes HOMO → LUMO, hence S_1, excitation corresponding to the electron density moving in the direction from the imine group toward the β-ionone ring, or the positive charge moving from the β-ionone ring toward the imine group. This is confirmed by analysis of the Mulliken charges (Table 4).

3.4. Other Torsional Angles. As discussed in the previous section, the twist in γ from planar (PSB11, $\gamma = 0°$) to perpendicular (AC, $\gamma \cong \pm 90°$) loosens the π-bond between the C_{11} and C_{12} atoms, leaving just a single σ-bond between the atoms in the AC regions. The unbound π-electrons switch over to the C_{10} and C_{13} atoms, turning the C_{10}−C_{11} and C_{12}−C_{13} bonds from single to double ones in character. This is clearly seen in the analysis of bond-length alternations over the retinal chain for the 11-cis → AC transition (Figure 7). The strengthening of the C_{10}−C_{11} and C_{12}−C13 bonds makes the torsional angles θ and ξ, neighboring γ, strictly planar, i.e., 180° at the AC ($\gamma \cong \pm 90°$) points.

Nevertheless, it was found that in areas near the barriers ($\gamma \cong \pm 45°$) on the $E_1(\gamma)$ minimum energy path, where the π-bonding ordering of the whole PSB structure is changing, θ and ξ show a moderate contribution to the reaction coordinate. In these areas, both θ and ξ deviate from planarity by up to ∼20°, in a direction opposite to the twist in γ, therefore trying to minimize the overall twist of the retinal chain. As soon as the π-bond between C_{11} and C_{12} is broken completely and the retinal system starts falling into one of the AC minima on the E_1 PES surface, neighboring single bonds turn into double bonds and θ and ξ quickly restore their planarity.

A separate series of calculations was performed to calculate the E_0 and E_1 PES curves as functions of θ and ξ.

Figure 9 shows the PES curves as functions of θ calculated with the B3LYP and CAM-B3LYP functionals for PSB11. Looking at the $E_0(\theta)$ energy curve it is seen that in addition to the PSB11 minimum, with θ in the trans-conformation, the $E_0(\theta)$ plots give us two other, higher in energy by ∼7 kcal/mol, minima with θ = 36° and 37° (CAM-B3LYP). These two minima correspond to the "curl-shaped" PSB11 structure found recently by Send and Sundholm[33] in their B3LYP calculations. The CAM-B3LYP barrier for adiabatic transition from the PSB11 S_0 conformation to the "curl-shaped" S_0 conformation is ∼12 kcal/mol. A similar picture was observed in B3LYP calculations, as seen from comparison of parts a (B3LYP) and b (CAM-B3LYP) of Figure 9. The barrier height is about half that calculated in the rigid B3LYP scan calculations reported by Send and Sundholm in ref 28. The major factor contributing to the barrier reduction is that the twist in θ is strongly coupled to the twist in the neighboring torsional angle γ.

The barrier for torsional rotation in θ for the first excited state is considerably smaller than for the ground state. Its value is 1.6−1.7 kcal/mol with TD DFT B3LYP and 1.1−1.2 kcal/mol with TD DFT CAM-B3LYP. The difference in B3LYP and CAM-B3LYP results is that the TD DFT B3LYP S_1 curve immediately falls in the conical intersection area after crossing the barrier, while the analogous TD DFT CAM-B3LYP S_1 curve, being higher in energy gives us, as in the case of twist in γ, the avoided crossing regions where it forms two additional S_1 minima. Therefore, the CAM-B3LYP results suggest that the PSB11 chromophore, after photoexcitation, may drift to those minima where it can stay for some time before relaxing to the ground state, or jumping to another minimum on the S_1 surface.

Another torsional angle neighboring the photoisomerization center is $\xi(C_{11}{=}C_{12}{-}C_{13}{=}C_{14})$. As such, it must be considered on equal footing with $\theta(C_9{=}C_{10}{-}C_{11}{=}C_{12})$. Figure 10 shows the S_0 and S_1 CAM-B3LYP PES calculated for PSB11 as

TABLE 3: Summary of B3LYP and CAM-B3LYP Energies (kcal/mol), Key Bond Distances (Å), and Torsion Angles (deg) for the Minima on the E_0 and E_1 Potential Energy Surfaces[a]

conformation	$r(C_{10},C_{11})$	$r(C_{11},C_{12})$	$r(C_{12},C_{13})$	ϕ	θ	γ	ξ	$E^{a,b}$	E^{c}
				B3LYP Results					
PSB11(S_0)	1.406	1.398	1.410	−31.9	179.8	0.2	−179.6	0.0	0.0
PSBT(S_0)	1.402	1.393	1.405	−30.8	179.8	179.9	−179.8	−5.3	−5.5
PSB11(S_1)	1.439	1.382	1.421	−90.0	−179.8	1.6	−178.7	35.1	35.4
PSBT(S_1)	1.435	1.379	1.416	−89.7	179.4	−179.7	179.7	29.8	29.5
				CAM-B3LYP Results					
PSB11(S_0)	1.408	1.387	1.409	−37.6	179.6	0.2	−179.7	0.0	0.0
PSBT(S_0)	1.404	1.383	1.403	−36.1	179.8	179.9	−179.9	−5.0	−5.2
PSB11(S_1)	1.414	1.391	1.415	−31.6	−176.8	10.7	−172.7	56.8	56.7
AC_1(S_1)	1.362	1.466	1.386	−36.3	177.4	92.7	179.2	40.1	41.2
AC_2(S_1)	1.362	1.466	1.386	−36.7	−177.8	−92.9	−179.1	40.1	41.2
PSBT(S_1)	1.414	1.384	1.413	−32.5	−179.8	−179.8	180.0	52.2	56.6

[a] Energies tabulated against the S_0 energy of 6-s-cis(−)-11-cis S_0 conformer. Geometries are optimized with the 6-31G(d) basis set. [b] Energy estimates with the 6-31G(d) basis set. [c] Energy estimates after single-point calculations with the 6-311G(2d,p) basis set.

TABLE 4: Mulliken Charge Distribution over the PSB Retinal Structure from TD DFT CAM-B3LYP Calculations for the Lowest Three Singlet States with Geometries Corresponding to the PSB11 S_0, PSB11 S_1, and AC S_1 Minima ($\gamma = -92.9°$)[a]

	geometry configuration								
	PSB11 S_0 minimum			PSB11 S_1 minimum			AC S_1 minimum		
	S_0	S_1	S_2	S_0	S_1	S_2	S_0	S_1	S_2
β-ionone	0.22	0.36	0.41	0.24	0.36	0.39	0.35	0.16	0.51
C_7	0.00	−0.02	−0.04	0.01	−0.02	−0.04	0.07	−0.04	−0.01
C_8	−0.02	0.01	0.00	−0.03	0.00	−0.01	−0.01	−0.02	0.01
C_9	0.24	0.19	0.21	0.24	0.19	0.22	0.30	0.14	0.23
C_{10}	−0.07	−0.03	−0.04	−0.07	−0.03	−0.04	0.02	0.01	0.03
C_{11}	0.08	0.02	0.02	0.09	0.03	0.03	0.09	−0.06	0.06
C_{12}	−0.07	−0.04	−0.04	−0.07	−0.04	−0.04	−0.16	0.04	−0.16
C_{13}	0.27	0.22	0.20	0.26	0.21	0.19	0.21	0.25	0.20
C_{14}	−0.07	−0.06	−0.06	−0.07	−0.06	−0.05	−0.12	0.00	−0.12
C_{15}	0.34	0.31	0.29	0.33	0.31	0.29	0.26	0.37	0.26
N	0.08	0.06	0.05	0.07	0.06	0.05	−0.01	0.15	−0.02
left of C_{11}=C_{12}	**0.45**	**0.52**	**0.55**	**0.47**	**0.52**	**0.55**	**0.82**	**0.19**	**0.83**
right of C_{11}=C_{12}	**0.55**	**0.48**	**0.45**	**0.53**	**0.48**	**0.45**	**0.18**	**0.81**	**0.17**
dipole shift[b]									
$\lvert\mu - \mu(S_0)\rvert$, Debye		**5.26**	**6.85**		**3.95**	**5.09**		**21.64**	**3.17**

[a] Charges on hydrogen atoms and methyl groups are added to the corresponding retinal PSB carbon atoms. [b] Relaxed, or correlated, densities[63,64] are used for the S_1 dipole calculations.

functions of ξ. The ground-state energy profile $E_0(\xi)$ has three minima: the lowest is in the middle $\xi = 180.3°$ and corresponds to the PSB11 stable conformation. Twisting the C_{12}−C_{13} bond can bring the system to either of the two local minima with $\xi \sim \pm 20°$. These minima are higher in energy by ∼2 kcal/mol than the PSB11 S_0 conformation. The S_0 barrier for the ξ twist ($\xi = 180.3° \rightarrow \xi \sim \pm 20°$) is ∼15 kcal/mol. The S_1 CAM-B3LYP PES produced in the relaxed scan along ξ is quite similar to the CAM-B3LYP S_1 PES produced in the relaxed scan along θ. It gives a barrier for falling from the PSB11 S_1 conformation to the AC(ξ) minima of ∼2 kcal/mol.

4. Conclusion

The strong deviation of TD DFT B3LYP results from analogous results obtained with the CAM-B3LYP functional, or with the CC2 method, shows the inadequacy of B3LYP for the treatment of the photoisomerization process in the retinal chromophore. As discussed in the Introduction, the failure of B3LYP in treatment of the excited states of the retinal structure is attributed to its incorrect asymptotic form of the exchange−correlation potential. As soon as the long-range asymptote of the exchange−correlation potential is corrected, as in the case of the CAM-B3LYP functional, TD DFT starts to produce results in agreement with more expensive CC2 calculations.[27,28]

A comparison of the B3LYP and CAM-B3LYP functionals in TD DFT calculations has been reported[29] recently by Send and Sundholm in application to some homologous model PSB's. The reason for the similarity between their B3LYP and CAM-B3LYP results is that the model molecules they studied do not have the ionone ring, which is the part of the system studied here that causes B3LYP and CAM-B3LYP to differ.

The S_0 and S_1 potential energy surfaces produced in TD DFT CAM-B3LYP calculations suggest the following path for the photoisomerization process:

−Initial vertical excitation of the PSB11 S_0 structure.

−Relaxation to the PSB11 S_1 local minimum.

−Torsional twist in γ, with ∼2 kcal/mol barrier, to the one of two AC minima with $\gamma \cong \pm 90°$. This twist weakens the π-bond between the C_{11} and C_{12} atoms causing a change in the order of single and double bonds in the region between the C_8 and C_{13} atoms of the retinal chain.

−De-excitation from the S_1 AC minimum to the S_0 surface with convergence to the global all-trans S_0 isomer. The precise path by which this last step occurs has not been determined, as the conical intersection on the surface has not been located.

It is interesting to look at the path taken on the excited-state surface. Figure 5 shows that from the geometry of the first excited state there is a comparatively low barrier of about 2

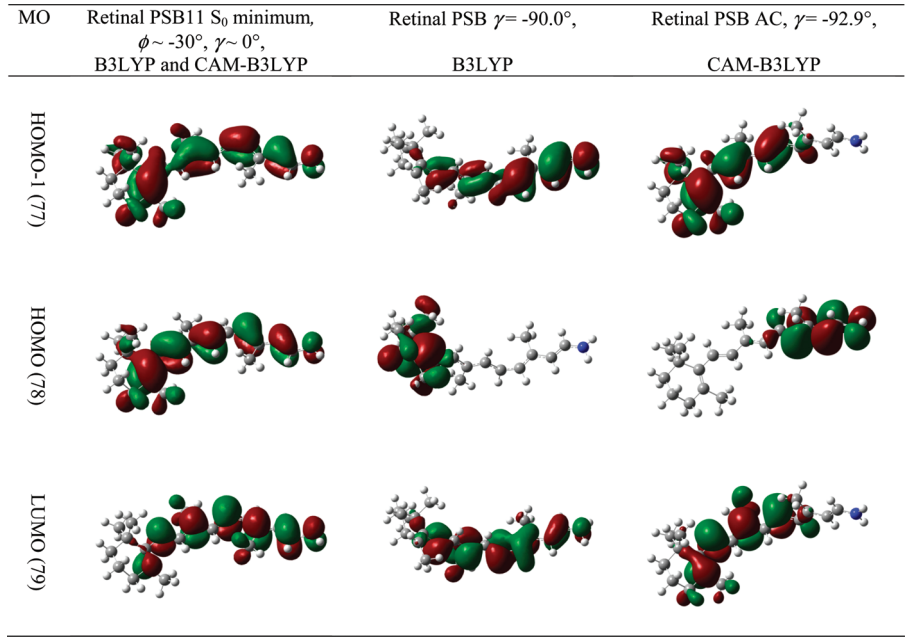

Figure 8. Graphical representation of molecular orbitals of the retinal PSB chromophore in the B3LYP and CAM-B3LYP calculations in regions with $\gamma \sim 0°$ and $\gamma \sim \pm 90°$.

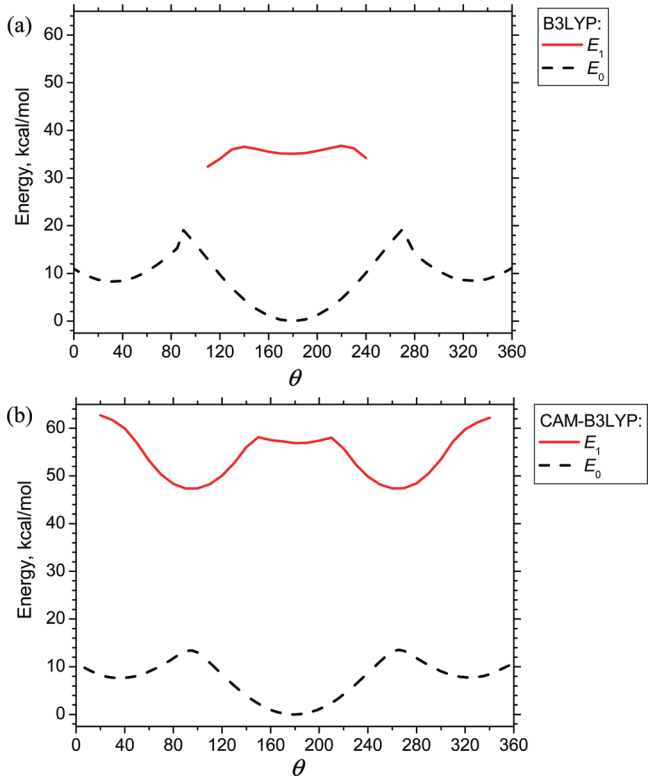

Figure 9. Potential-energy curves for the ground (E_0) and first excited (E_1) states of PSB11 as functions of the θ angle calculated at the DFT (E_0) and TD DFT (E_1) levels with an interval of 10° using the B3LYP (a) and CAM-B3LYP (b) functionals.

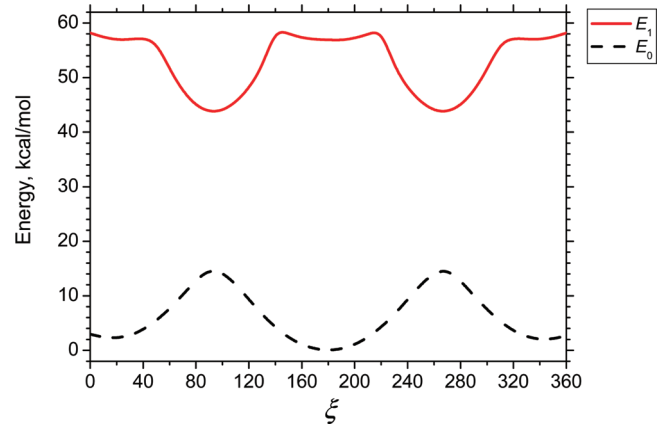

Figure 10. Potential-energy curves for the ground (E_0) and first excited (E_1) states of PSB11 as functions of the ξ angle calculated at the DFT (E_0) and TD DFT (E_1) levels with interval of 10° using the CAM-B3LYP functional.

kcal/mol. To reach this barrier requires only a small twist of the angle γ, accompanied by a rearrangement of the bonds. As soon as the barrier is crossed, the C_{11}—C_{12} bond, as can be seen clearly from Figure 6, effectively becomes a single rather than a double bond. Thus the rotation in γ does not break the double bond; rather, it causes the bond to rearrange to neighboring positions. This feature can only be seen if one fully relaxes the other coordinates as the angle γ is varied—a rigid rotation would not reveal the critical nature of the coupling between changes in the angle and the bond lengths. The present calculations suggest that it is this coupling that results in the relatively low energy path from the first excited state back toward the conical intersection. The B3LYP calculations do not show this feature, even with fully relaxed geometries. The CC2 calculations of Send and Sundholm have a significantly higher barrier for rotation of γ, as the bond lengths are not varied.

The results of the TD DFT CAM-B3LYP S_1 relaxed scan along the bond torsional angles neighboring C_{11}=C_{12} (Figures 8b and 9) show that a perpendicular twist of either the C_{10}—C_{11} or C_{12}—C_{13} bond on the S_1 PSB11 PES surface is as easy as the perpendicular twist of the C_{11}=C_{12} bond. The values of barrier for either of these perpendicular twists lie in a range 1.5−2 kcal/mol. However, the most probable output after the perpendicular twist of the C_{10}—C_{11} or C_{12}—C_{13} bond and de-excitation to the S_0 PES would be return to the PSB11 conformation, as it is lower in energy than the "curled" conformations forming some extra local minima on the S_0 PSB11 energy surface. Figures 9 and 10 imply that there are several of these "curled" configurations.

These calculations show that the CAM-B3LYP functional avoids the difficulties met by other authors in TD DFT calculations of the excited-state energy profiles for the protonated Schiff-base retinal.[28] This suggests the TD DFT method in combination with the CAM-B3LYP potential to be a useful tool for theoretical studies of the retinal chromophore photoisomerization process.

References and Notes

(1) Shichi, H. *Biochemistry of Vision*; Academic Press: New York, 1983.

(2) Filipek, S.; Teller, D. C.; Palczewski, K.; Stenkamp, R. *Annu. Rev. Biophys. Biomol. Struct.* **2003**, *32*, 375.

(3) Schoenlein, R. W.; Peteanu, L. A.; Mathies, R. A.; Shank, C. V. *Science* **1991**, *254*, 412.

(4) Peteanu, L. A.; Schoenlein, R. W.; Wang, Q.; Mathies, R. A.; Shank, C. V. *Proc. Natl. Acad. Sci. U.S.A.* **1993**, *90*, 11762.

(5) Wang, Q.; Schoenlein, R. W.; Peteanu, L. A.; Mathies, R. A.; Shank, C. V. *Science* **1994**, *266*, 422.

(6) Wang, Q.; Kochendoerfer, G. G.; Schoenlein, R. W.; Verdegem, P. J. E.; Lugtenburg, J.; Mathies, R. A.; Shank, C. V. *J. Phys. Chem.* **1996**, *100*, 17388.

(7) Kukura, P.; McCamant, D. W.; Yoon, S.; Wandschneider, D. B.; Mathies, R. A. *Science* **2005**, *310*, 1006.

(8) McCamant, D. W.; Kukura, P.; Mathies, R. A. *J. Phys. Chem. B* **2005**, *109*, 10449.

(9) Kukura, P.; Yoon, S.; Mathies, R. A. *Anal. Chem.* **2006**, *78*, 5952.

(10) Kim, J. E.; McCamant, D. W.; Zhu, L. Y.; Mathies, R. A. *J. Phys. Chem. B* **2001**, *105*, 1240.

(11) Delaney, J. K.; Schmidt, P. K.; Brack, T. L.; Atkinson, G. H. *J. Phys. Chem. B* **2000**, *104*, 10827.

(12) Terentis, A. C.; Ujj, L.; Abramczyk, H.; Atkinson, G. H. *Chem. Phys.* **2005**, *313*, 51.

(13) Akiyama, R.; Kakitani, T.; Imamoto, Y.; Shichida, Y.; Hatano, Y. *J. Phys. Chem.* **1995**, *99*, 7147.

(14) Kandori, H.; Shichida, Y.; Yoshizawa, T. *Biophys. J.* **1989**, *56*, 453.

(15) Popp, A.; Ujj, L.; Atkinson, G. H. *J. Phys. Chem.* **1995**, *99*, 10043.

(16) Green, B. H.; Monger, T. G.; Alfano, R. R.; Aton, B.; Callender, R. H. *Nature* **1977**, *269*, 179.

(17) Yan, M.; Manor, D.; Weng, G.; Chao, H.; Rothberg, L.; Jedju, T. M.; Alfano, R. R.; Callender, R. H. *Proc. Natl. Acad. Sci. U.S.A.* **1991**, *88*, 9809.

(18) Casida, M. E. In *Recent advances in Density Functional Theory Methods*; Chong, D. P., Ed.; World Scientific: Singapore, 1995; Part 1.

(19) Bauernschmitt, R.; Ahlrichs, R. *Chem. Phys. Lett.* **1996**, *256*, 454.

(20) Wanko, M.; Garavelli, M.; Bernardi, F.; Niehaus, T. A.; Frauenheim, T.; Elstner, M. *J. Chem. Phys.* **2004**, *120*, 1674.

(21) Andruniow, T.; Ferre, N.; Olivucci, M. *Proc. Natl. Acad. Sci. U.S.A.* **2004**, *101*, 17908.

(22) Frutos, L. M.; Andruniow, T.; Santoro, F.; Ferre, N.; Olivucci, M. *Proc. Natl. Acad. Sci. U.S.A.* **2007**, *104*, 7764.

(23) Ishida, T.; Nanbu, S.; Nakamura, H. *J. Phys. Chem. A* **2009**, *113*, 4356.

(24) Aquino, A. J. A.; Barbatti, M.; Lischka, H. *Chemphyschem* **2006**, *7*, 2089.

(25) Szymczak, J. J.; Barbatti, M.; Lischka, H. *J. Chem. Theory Comput.* **2008**, *4*, 1189.

(26) Szymczak, J. J.; Barbatti, M.; Lischka, H. *J. Phys. Chem. A* **2009**, *113*, 11907.

(27) Send, R.; Sundholm, D. *Phys. Chem. Chem. Phys.* **2007**, *9*, 2862.

(28) Send, R.; Sundholm, D. *J. Phys. Chem. A* **2007**, *111*, 8766.

(29) Send, R.; Sundholm, D.; Johansson, M. P.; Pawlowski, F. *J. Chem. Theory Comput.* **2009**, *5*, 2401.

(30) Wanko, M.; Hoffmann, M.; Strodet, P.; Koslowski, A.; Thiel, W.; Neese, F.; Frauenheim, T.; Elstner, M. *J. Phys. Chem. B* **2005**, *109*, 3606.

(31) Altun, A.; Yokoyama, S.; Morokuma, K. *J. Phys. Chem. A* **2009**, *113*, 11685.

(32) Send, R.; Sundholm, D. *J. Phys. Chem. A* **2007**, *111*, 27.

(33) Send, R.; Sundholm, D. *J. Mol. Model.* **2008**, *14*, 717.

(34) Wanko, M.; Hoffmann, M.; Frauenheim, T.; Elstner, M. *J. Comput. Aided Mol. Des.* **2006**, *20*, 511.

(35) Altun, A.; Yokoyama, S.; Morokuma, K. *J. Phys. Chem. B* **2008**, *112*, 16883.

(36) Altun, A.; Yokoyama, S.; Morokuma, K. *J. Phys. Chem. B* **2008**, *112*, 6814.

(37) Van Caillie, C.; Amos, R. D. *Chem. Phys. Lett.* **1999**, *308*, 249.

(38) Van Caillie, C.; Amos, R. D. *Chem. Phys. Lett.* **2000**, *317*, 159.

(39) Becke, A. D. *J. Chem. Phys.* **1993**, *98*, 5648.

(40) Stephens, P. J.; Jalkanen, K. J.; Devlin, F. J.; Chabalowski, C. F. *J. Phys. Chem.* **1993**, *97*, 6107.

(41) Handy, N. C. *Mol. Phys.* **2004**, *102*, 2399.

(42) Tawada, Y.; Tsuneda, T.; Yanagisawa, S.; Yanai, T.; Hirao, K. *J. Chem. Phys.* **2004**, *120*, 8425.

(43) Bonacickoutecky, V.; Kohler, J.; Michl, J. *Chem. Phys. Lett.* **1984**, *104*, 440.

(44) Bonacickoutecky, V.; Schoffel, K.; Michl, J. *Theor. Chim. Acta* **1987**, *72*, 459.

(45) Gonzalez-Luque, R.; Garavelli, M.; Bernardi, F.; Merchan, M.; Robb, M. A.; Olivucci, M. *Proc. Natl. Acad. Sci. U.S.A.* **2000**, *97*, 9379.

(46) Yanai, T.; Tew, D. P.; Handy, N. C. *Chem. Phys. Lett.* **2004**, *393*, 51.

(47) Kobayashi, R.; Amos, R. D. *Chem. Phys. Lett.* **2006**, *420*, 106.

(48) Cai, Z. L.; Crossley, M. J.; Reimers, J. R.; Kobayashi, R.; Amos, R. D. *J. Phys. Chem. B* **2006**, *110*, 15624.

(49) Yin, S.; Dahlbom, M. G.; Canfield, P. J.; Hush, N. S.; Kobayashi, R.; Reimers, J. R. *J. Phys. Chem. B* **2007**, *111*, 9923.

(50) Peach, M. J. G.; Helgaker, T.; Salek, P.; Keal, T. W.; Lutnaes, O. B.; Tozer, D. J.; Handy, N. C. *Phys. Chem. Chem. Phys.* **2005**, *8*, 558.

(51) Rudberg, E.; Salek, P.; Helgaker, T.; Agren, H. *J. Chem. Phys.* **2005**, *123*, 184108.

(52) Coto, P. B.; Sinicropi, A.; De Vico, L.; Ferre, N.; Olivucci, M. *Mol. Phys.* **2006**, *104*, 983.

(53) Gascon, J. A.; Batista, V. S. *Biophys. J.* **2004**, *87*, 2931.

(54) Gascon, J. A.; Sproviero, E. M.; Batista, V. S. *Acc. Chem. Res.* **2006**, *39*, 184.

(55) Rohrig, U. F.; Guidoni, L.; Rothlisberger, U. *Chemphyschem* **2005**, *6*, 1836.

(56) Leenders, E. J. M.; Guidoni, L.; Rothlisberger, U.; Vreede, J.; Bolhuis, P. G.; Meijer, E. J. *J. Phys. Chem. B* **2007**, *111*, 3765.

(57) Okada, T.; Sugihara, M.; Bondar, A. N.; Elstner, M.; Entel, P.; Buss, V. *J. Mol. Biol.* **2004**, *342*, 571.

(58) Vreven, T.; Morokuma, K. *Theor. Chem. Acc.* **2003**, *109*, 125.

(59) Becke, A. D. *Phys. Rev. A* **1988**, *38*, 3098.

(60) Vosko, S. H.; Wilk, L.; Nusair, M. *Can. J. Phys.* **1980**, *58*, 1200.

(61) Lee, C. T.; Yang, W. T.; Parr, R. G. *Phys. Rev. B* **1988**, *37*, 785.

(62) Frisch, M. J.; Trucks, G. W.; Schlegel, H. B.; Scuseria, G. E.; Robb, M. A.; Cheeseman, J. R.; Montgomery, J. A., Jr.; Vreven, T.; Scalmani, G.; Mennucci, B.; Barone, V.; Petersson, G. A.; Caricato, M.; Nakatsuji, H.; Hada, M.; Ehara, M.; Toyota, K.; Fukuda, R.; Hasegawa, J.; Ishida, M.; Nakajima, T.; Honda, Y.; Kitao, O.; Nakai, H.; Li, X.; Hratchian, H. P.; Peralta, J. E.; Izmaylov, A. F.; Kudin, K. N.; Heyd, J. J.; Brothers, E.; Staroverov, V.; Zheng, G.; Kobayashi, R.; Normand, J.; Sonnenberg, J. L.; Ogliaro, F.; Bearpark, M.; Parandekar, P. V.; Ferguson, G. A.; Mayhall, N. J.; Iyengar, S. S.; Tomasi, J. ; Cossi, M.; Rega, N.; Burant, J. C.; Millam, J. M.; Klene, M.; Knox, J. E.; Cross, J. B.; Adamo, C.; Jaramillo, J.; Gomperts, R.; Stratmann, R. E.; Yazyev, O.; Austin, A. J.; Cammi, R.; Pomelli, C.; Ochterski, J. W.; Ayala, P. Y.; Morokuma, K.; Voth, G. A.; Salvador, P.; Dannenberg, J. J.; Zakrzewski, V. G.; Dapprich, S.; Daniels, A. D.; Strain, M. C.; Farkas, O.; Malick, D. K.; Rabuck, A. D.; Raghavachari, K.; Foresman, J. B.; Ortiz, J. V.; Cui, Q.; Baboul, A. G.; Clifford, S.; Cioslowski, J.; Stefanov, B. B.; Liu, G.; Liashenko, A.; Piskorz, P.; Komaromi, I.; Martin, R. L.; Fox, D. J.; Keith, T. ; Al-Laham, M. A.; Peng, C. Y.; Nanayakkara, A.; Challacombe, M.; Chen, W.; Wong, M. W.; Pople, J. A. *Gaussian Development Version*, Revision G.01; Gaussian Inc.: Wallingford, CT, 2007.

(63) Wiberg, K. B.; Hadad, C. M.; Lepage, T. J.; Breneman, C. M.; Frisch, M. J. *J. Phys. Chem.* **1992**, *96*, 671.

(64) Amos, R. D. *Chem. Phys. Lett.* **2002**, *364*, 612.

(65) Nielsen, I. B.; Lammich, L.; Andersen, L. H. *Phys. Rev. Lett.* **2006**, *96*, 018304.

(66) Kandori, H.; Katsuta, Y.; Ito, M.; Sasabe, H. *J. Am. Chem. Soc.* **1995**, *117*, 2669.

(67) Arnaboldi, M.; Motto, M. G.; Tsujimoto, K.; Baloghnair, V.; Nakanishi, K. *J. Am. Chem. Soc.* **1979**, *101*, 7082.

(68) Sekharan, S.; Weingart, O.; Buss, V. *Biophys. J.* **2006**, *91*, L7.

(69) Ponder, M.; Mathies, R. *J. Phys. Chem.* **1983**, *87*, 5090.

JP911329G